New insights in the spatially resolved dynamic pH measurement in macroscopic large absorbent particles by confocal laser scanning microscopy

Heinemann, Matthias; Limper, Uta; Büchs, Jochen

Published in:
Journal of Chromatography A

DOI:
10.1016/j.chroma.2003.09.065

Publication date:
2004

Available online at www.sciencedirect.com
SCIENCE DIRECT®
Journal of Chromatography A, 1024 (2004) 45–53
JOURNAL OF CHROMATOGRAPHY A
www.elsevier.com/locate/chroma

New insights in the spatially resolved dynamic pH measurement in macroscopic large absorbent particles by confocal laser scanning microscopy

Matthias Heinemann*, Uta Limper, Jochen Büchs

Biochemical Engineering, RWTH Aachen University, Worringer Weg 1, 52056 Aachen, Germany

Received 22 April 2003; received in revised form 9 September 2003; accepted 23 September 2003

Abstract

Both, experimental investigation of protein adsorption processes and mathematical models describing such processes indicate, that the pH in the absorbent particle might be the key factor for an improved understanding of these chromatographic processes. Thus, a technique aiming at the spatially resolved pH measurement in macroscopic large absorbent particles is presented. The first application of this method, being based on confocal laser scanning microscopy (CLSM), revealed an apparent dependence of the pH calibration curve on the scanning depth. By a model-based approach, factors distorting the measurement signal are identified: The wavelength-dependent light scattering and the re-absorption of emitted light. The resulting consequences for further development and application of CLSM based techniques to measure pH in macroscopic large absorbent particles are illustrated and discussed.

Keywords: Protein chromatography; pH imaging; Confocal laser scanning microscopy; Absorbent particles

1. Introduction

Confocal laser scanning microscopes (CLSM) have been widely used for spatially resolved determination of protein concentrations inside various carrier matrices and absorbent particles of macroscopic size [1–10]. Dynamic protein absorption experiments, recently observed with confocal laser scanning microscopes, revealed unexpected protein concentration profiles, the so-called concentration rings [5,7,10]. These inner radial humps, however, cannot be reproduced, to the best of our knowledge, by existing mathematical models based on the traditional theories of protein absorption [11–14]. Recently, a first mathematical model was developed which now allows at least for a qualitative representation of the experimentally observed concentration rings [15,16]. In contrast to the traditional models, this model also takes into account electrical double layer interactions inside the absorbent particle. In addition, it was experimentally observed that concentration rings only occur under certain conditions of pH and ionic strength [5,10]. Together with the fact that also another theoretical model demonstrated that non-uniform distributions of pH may exist during the protein absorption process [17], the pH in the absorbent particle seems to be a key factor for the understanding of such chromatographic processes. However, for deeper insights and for a further improvement of the newly developed model describing the concentration rings, information about the dynamic behavior of the pH in the absorbent particle is imperative and thus, suitable measurement techniques are required.

In the context of spatially resolved pH measurement, confocal laser scanning microscopes have been successfully employed at the scale of biological cells [18–22]. The successful application of CLSM based techniques for measuring pH in living biological cells raised great expectations to use confocal laser scanning microscopes also for a non-invasive and spatially resolved pH measurement in carrier matrices and absorbent particles of macroscopic size [23]. A first transfer of CLSM based pH measurement techniques from the scale of biological cells to macroscopic large objects was

* Corresponding author. Fax: +49-241-8022265.
E-mail address: heinemann@biovt.rwth-aachen.de (M. Heinemann).

0021-9673/$ – see front matter © 2003 Elsevier B.V. All rights reserved.
doi:10.1016/j.chroma.2003.09.065

undertaken by Spiess and Kasche [24]. For their pH measurement technique, two fluorescent dyes were introduced into a number of different porous particles. The fluorescent dyes, being attached to enzymes present in the particle, consisted of a pH-sensitive dye (fluoresceinisothiocyanate) and a pH-insensitive dye (tetramethylrhodaminisothiocyanate). The measured intensity signal of the pH-sensitive dye was normalized with the signal of the pH-insensitive dye. By the application of this technique, the authors stated that they were able to observe pH gradients in the particles. However, an unexplainable dependence of the pH calibration curve on the scanning depth was reported by the authors.

Within our work, a different CLSM based approach was pursued towards the spatially resolved pH measurement in porous particles. Here, alginate beads [25,26] were employed as a model for various carrier matrices. (The polysaccharide alginate forms hydrogels with bivalent cations.) In contrast to the work of Spiess and Kasche [24], the here developed measurement technique requires only a single fluorescent dye. This is due to the fact that the employed fluorescent dye exhibits pH-dependent dual-emission spectra which allow for a normalization of the pH-dependent response in terms of the ratio of two fluorescence intensities measured at different wavelengths. Dual-emission ratiometry eliminates potential distortions of the measurement being possible with the application of two dyes. Such distortions can be caused, for example, by different rates of photobleaching or by variations in probe loading [27]. However, despite the utilization of a less fault-prone technique, also here a dependence of the pH calibration curve of the scanning depth was observed.

This up to now unexplainable phenomenon, which occurred independently with two different methods, is obviously only attributed to the spatially resolved pH measurement in macroscopic large objects, since, to the best of our knowledge, a scanning depth dependence of intensity ratios has not been observed in CLSM based ratiometric pH measurements in biological cells. However, for a reliable CLSM based measurement of spatially resolved pH values in macroscopic large objects such as absorbent particles, it is imperative to know the phenomena, which have an impact on the measured intensity signals. Only in this case, the measured signals can be properly corrected for perturbing factors. Otherwise, biased results with systematic errors would subsequently lead to wrong conclusions.

Therefore, this work provides new fundamental understanding of spatially resolved pH measurement in macroscopic large absorbent particles by confocal laser scanning microscopes. After a short outline of the here developed measurement technique and the presentation of the obtained depth dependent calibration curve, factors distorting the measurement signal are identified by a model-based approach. Subsequently, the resulting consequences for a further development and future application of CLSM based techniques to measure pH in macroscopic large absorbent particles are illustrated and discussed.

2. Experimental

2.1. Fluorescent dye

The pH-sensitive indicator SNARF-4F 5-(and-6)-carboxylic acid which exhibits dual-emission properties was purchased from Molecular Probes (Leiden, The Netherlands). The dye has a pKa of approximately 6.4 and therefore allows for pH measurement between pH 7.5 and 5 [28].

2.2. Preparation of alginate beads

Ten milliliter of a buffered (100 mM 2-(*N*-morpholino)-ethanesulfonic acid (MES), 20 mM Tris-(hydroxymethyl)-aminomethane (TRIS)) 2% (w/v) alginate solution and 90 ml of an equally buffered 2% (w/v) $CaCl_2$ solution were prepared. Both solutions contained 4 μM of SNARF-4F. To form the gel beads, the highly viscous alginate solution was dropped (with a syringe) into the buffered $CaCl_2$ solution (hardening bath), resulting in beads with a diameter between 1.7 and 2 mm. The hardening bath, containing the beads, was then divided in eight aliquots. Each aliquot was subsequently adjusted to a different pH value (pH 7.5, 7.0, 6.5, 6.0, 5.75, 5.5, 5.25, 5.0) by the addition of either NaOH (2 M) or HCl (1 M). The pH adjustment was done in a number of small steps over several hours to allow the titrated acid or base to diffuse into the alginate matrix and to equilibrate the intra-bead pH with the controlled pH in the hardening bath. The titration process was continued until the pH value in the hardening bath remained constant. Due to the different titration volumes of NaOH and HCl, the final dye concentrations in the aliquots (beads and liquid) were all slightly different. After 12 h in the hardening bath, the beads were removed with a filter, shortly dried with a paper towel and transferred into a water saturated hexane solution. Because of the insolubility of the dye in hexane, a leakage of the dye from the aqueous beads to the hexane phase was prevented. The samples were protected against light exposure.

2.3. Determination of spectra

Fluorescence emission spectra of SNARF-4F solutions were recorded with a spectrofluorimeter SLM-Aminco Bowman Series 2 (Thermo Spectronic, Rochester, USA). Absorption spectra were determined with a spectrophotometer Uvikon 992 A (Kontron Instruments, Milan, Italy).

2.4. Instrumentation and microscope settings

The experiments were performed with an upright confocal laser scanning microscope TCS SP from Leica (Heidelberg, Germany) equipped with an argon/krypton laser. A 10× water immersion objective (Leica HCX APO, L10x/0.30 W,

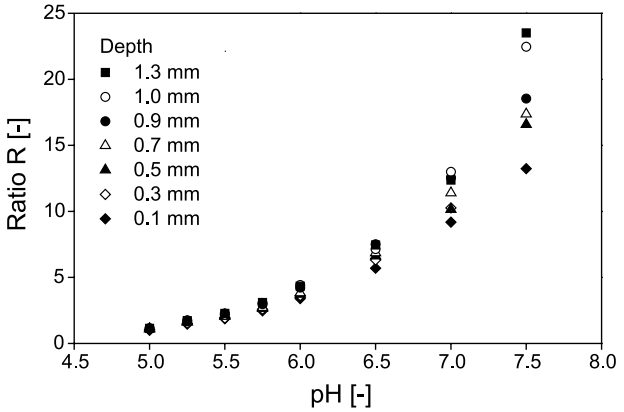

Fig. 1. Intensity ratios as a function of pH and scanning depth obtained from *z*-scanning alginate beads which were adjusted to various pH values.

Germany, Heidelberg) with a working distance of 3.7 mm was used for the experiments.[1] This objective allowed a field of view of 1.0 mm × 1.0 mm. The images were recorded at a resolution of 512 × 512 pixels and were analyzed by the supplied Leica Confocal Software (version 2.477, Germany, Heidelberg).

The fluorescent dye was excited at 568 nm. As suitable pair of wavelengths for the ratiometric pH determination, the collection windows between 585 and 590 nm and 660 and 665 nm were selected for detection. Collection windows of 5 nm were necessary to avoid insufficient light. The beamsplitter RT 30/70 (neutral filter) was selected for the analysis.

2.5. Confocal analysis

For the confocal analysis, a single alginate bead, which contained the fluorescent dye, was placed in a chamber (filled with hexane) on a horizontally aligned nylon net situated in the middle of the chamber. By this, reflections between the bead and the bottom glass of the chamber were prevented. The water immersion objective was immersed in the hexane solution and the emitted light was collected from the top. By this setup, distortions caused by refractions of the light were minimized, resulting in an improved overall collection efficiency, which is dependent on the index of refraction between the objective lens and the source. As in our experiments, hexane and the alginate bead (consisting of 98% water) were between the objective and the source and the index of refraction of water (1.333) is almost identical to that of hexane (1.372), the overall collection efficiency can be considered to remain constant, when different depth positions inside the carrier are focussed.

[1] In confocal microscopy, the theoretical lateral resolution of an objective lens (R_l) can be approximated by $R_l = (0.46\lambda)/\mathrm{NA}$ and the theoretical axial resolution (R_a) by $R_a = (1.4n\lambda)/(\mathrm{NA})^2$, where NA is the numerical aperture of the objective, λ the wavelength of the detected light and n the refractive index of the mount medium [29]. The set-up in this study gives a theoretical lateral resolution of ∼1 μm and a theoretical axial resolution of ∼14 μm.

In this work, the confocal measurements were conducted with the *z*-scan mode. With this mode, a series of (*xy*) optical sections across the specimen in a plane perpendicular to the optical axis (*z*-direction) is collected. The result is a stack of images, each corresponding to a certain *z* position. In the center of the obtained images, a small area (0.04 mm^2) is selected and the mean fluorescent intensity of this area is determined. A step length (in *z*-direction) of 100 μm was used within this work.

3. Results

3.1. Observation of an apparent scanning depth dependence of the ratiometric signal

A number of alginate beads, each adjusted to a different pH value, were scanned with the *z*-scan mode while the fluorescence intensities were recorded at the two selected collection windows. Before the calculation of intensity ratios, the measured fluorescence intensities were corrected for the background noise of the detector. The intensity of the background noise was determined in the hexane phase which surrounded the alginate bead and which did not contain any fluorescent dye because of the dye's insolubility in the organic solvent. The intensity ratios defined as the fluorescence intensity between 660 and 665 nm divided by the fluorescence intensity between 585 and 590 nm, obtained from different scanning depths, are presented in Fig. 1 as a function of pH. It is obvious from this figure, that the obtained ratios are not only dependent on pH but apparently also on the path length of the light through the opaque alginate matrix. With increasing length of the light path, the intensity ratio increases. This result demonstrates, that also with the here applied method, a scanning depth dependence of the ratiometric signal is obtained, just as it has been observed with the method developed by Spiess and Kasche [24].

3.2. Investigation on the factors influencing the ratiometric measurement

In the following, the unknown reasons for the observed scanning depth dependence of the ratiometric signal are investigated. The factors potentially influencing the ratiometric measurement are examined by a model-based analysis of the obtained experimental data. Therefore, at first, mathematical models with varying underlying hypotheses are developed. A subsequent comparison of experimental results with predictions from different models allows to discriminate between competing models and thus to identify factors negatively influencing the measurement signal.

Respective mathematical models have to take into account factors which determine the transformation of the original exciting light $I_{ex}^{(0)}$ into the two actually measured intensities of the emitted light, $I_{662.5}^{(0)}$ and $I_{587.5}^{(0)}$. Some factors influence the two emitted light intensities to the

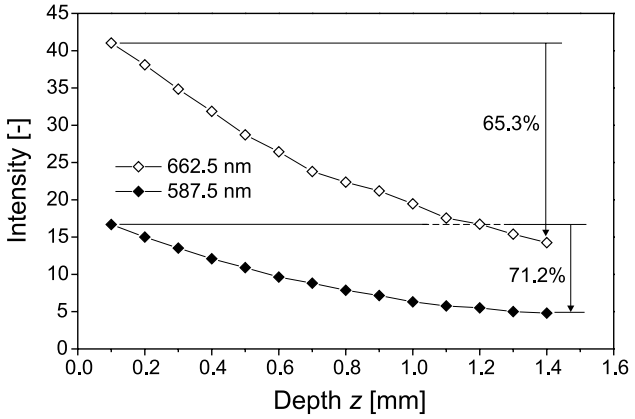

Fig. 2. Intensities measured at two wavelengths as a function of the scanning depth (alginate bead adjusted to pH 5.75).

same extent. Consequently, the ratio $R^{(0)}$ of these light intensities is not affected. Other factors, in contrast, are dependent on the wavelength of the light and thus the ratio $R^{(0)}$ is influenced. Such a phenomenon is, for example, the wavelength-dependent attenuation of light [30–32].

3.2.1. Hypothesis 1: wavelength-dependent attenuation of light

When scanning an alginate bead with the *z*-scan mode, the intensities of the detected fluorescence signals decrease with increasing scanning depth [6]. This is also obvious from the intensity profiles presented in Fig. 2. This figure additionally demonstrates that the degree of light attenuation is apparently dependent on the wavelength of the emitted light. Here, over the length of 1.3 mm, the light intensity at 587.5 nm is reduced by 71.2% whereas the light intensity at 662.5 nm is only cut down by 65.3%. The light attenuation is caused by a wavelength-dependent scattering of the light off the slightly opaque alginate matrix. This scattering has been described as Rayleigh effect which was initially observed with air molecules, but which also occurs with macromolecules [33] such as the polysaccharides of the alginate matrix. The attenuation of light by Rayleigh scattering is proportional to the wavelength λ according to $1/\lambda^4$ [34]. This means that a higher light attenuation occurs at lower wavelengths. This is in good agreement with the observation illustrated in Fig. 2. The different degrees of light attenuation here result in raising intensity ratios with increasing scanning depth. Thus, a first mathematical model was developed which includes wavelength-dependent light attenuation. Generally, the model equations would have to take into account the conical shape of the excitation and emission light beam [30,31]. However, here, an objective with a very low numerical low aperture was employed which means that a very acute light cone is obtained (semi-angle: 13°). For this reason and also because a spherical object was examined, the path lengths of the light rays through the bead (e.g. at the outside and in the center of the cone) can be considered to be identical (within the measurement accuracy). Therefore, each light ray undergoes the same light attenuation and thus it is justified to derive the model equations only for the beam in the middle of the light cone. In the following, the proposed model is presented. For illustrating purposes, the model equations are additionally compiled in Fig. 3.

The original, non-attenuated exciting laser light (intensity $I_{ex}^{(0)}$) passes through the opaque alginate matrix and reaches the focussed optical slice at depth z_s. On its way, the light is

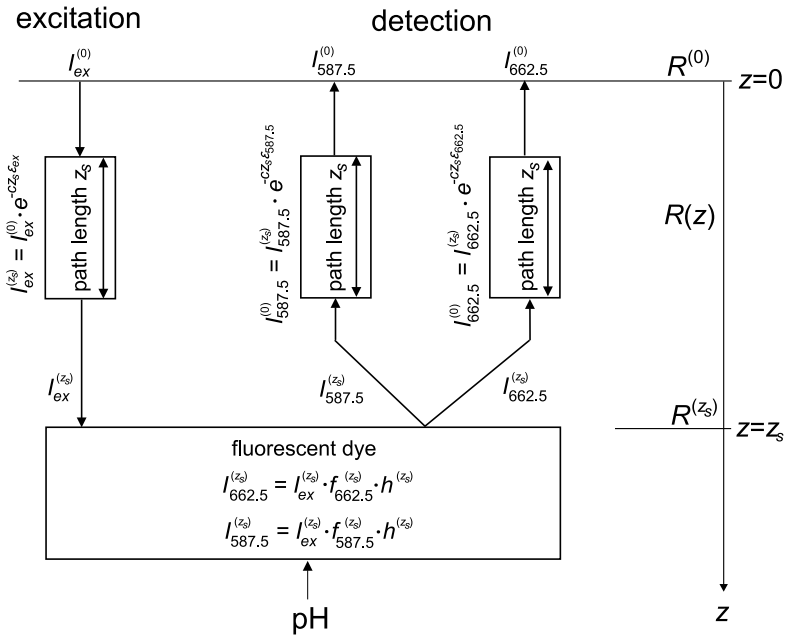

Fig. 3. Presentation of model equations.

attenuated. The residual intensity of the exciting light at the scanning depth, $I_{ex}^{(z_s)}$, is determined by the Lambert–Beer law according to:

$$I_{ex}^{(z_s)}(z_s) = I_{ex}^{(0)}\, e^{-c\varepsilon_{ex}(z_s-0)} \quad (1)$$

where ε_{ex} represents the absorptivity coefficient at the wavelength of the exciting light, $(z_s - 0)$ the path length of the light through the alginate bead and c the concentration of the absorbing species (here, alginate molecules).

The light intensity emitted by the fluorophore is dependent on the intensity of the excitation light $I_{ex}^{(z_s)}$ at the scanning depth z_s, on the pH, on microscopic parameters and on characteristics of the fluorophore [21]. For modeling purposes, here, the pH-dependent light emission of the dye at the two distinct wavelengths is described with the functions $f_{587.5}^{(z_s)}$ and $f_{662.5}^{(z_s)}$. The microscopic and fluorophore parameters are incorporated in the function $h^{(z_s)}$. Thus, the emitted fluorescence intensities at the scanning depth z_s, $I_{587.5}^{(z_s)}$ and $I_{662.5}^{(z_s)}$, can be calculated by the following equations:

$$I_{587.5}^{(z_s)}(\mathrm{pH}, z_s) = I_{ex}^{(z_s)}(z_s) f_{587.5}^{(z_s)}(\mathrm{pH}) h^{(z_s)}(\dots) \quad (2)$$

$$I_{662.5}^{(z_s)}(\mathrm{pH}, z_s) = I_{ex}^{(z_s)}(z_s) f_{662.5}^{(z_s)}(\mathrm{pH}) h^{(z_s)}(\dots) \quad (3)$$

The intensities of the emitted light, $I_{587.5}^{(z_s)}$ and $I_{662.5}^{(z_s)}$, are also attenuated on their way through the alginate matrix according to the Lambert–Beer law. The degree of light attenuation is dependent on the wavelength of the light, which is expressed by different absorptivity coefficients $\varepsilon_{587.5}$ and $\varepsilon_{662.5}$. The finally detected fluorescence intensities, $I_{587.5}^{(0)}$ and $I_{662.5}^{(0)}$, are given by the following equations:

$$I_{587.5}^{(0)}(\mathrm{pH}, z_s) = I_{587.5}^{(z_s)}(\mathrm{pH}, z_s)\, e^{-c\varepsilon_{587.5} z_s} \quad (4)$$

$$I_{662.5}^{(0)}(\mathrm{pH}, z_s) = I_{662.5}^{(z_s)}(\mathrm{pH}, z_s)\, e^{-c\varepsilon_{662.5} z_s} \quad (5)$$

By rearranging the so far presented equations, the following correlations for the detected light intensities, $I_{587.5}^{(0)}$ and $I_{662.5}^{(0)}$, are obtained:

$$I_{587.5}^{(0)}(\mathrm{pH}, z_s) = I_{ex}^{(0)} f_{587.5}^{(z_s)}(\mathrm{pH}) h^{(z_s)}(\dots)\, e^{-c(\varepsilon_{ex}+\varepsilon_{587.5}) z_s} \quad (6)$$

$$I_{662.5}^{(0)}(\mathrm{pH}, z_s) = I_{ex}^{(0)} f_{662.5}^{(z_s)}(\mathrm{pH}) h^{(z_s)}(\dots)\, e^{-c(\varepsilon_{ex}+\varepsilon_{662.5}) z_s} \quad (7)$$

The ratio $R^{(0)}$ between the two detected intensities, $I_{587.5}^{(0)}$ and $I_{662.5}^{(0)}$, representing a normalized measure for pH, is given by dividing Eq. (7) by Eq. (6):

$$R^{(0)}(\mathrm{pH}, z_s) = \frac{I_{662.5}^{(0)}(\mathrm{pH}, z_s)}{I_{587.5}^{(0)}(\mathrm{pH}, z_s)} = \frac{f_{662.5}^{(0)}(\mathrm{pH})}{f_{587.5}^{(0)}(\mathrm{pH})}\, e^{-c(\varepsilon_{662.5}-\varepsilon_{587.5}) z_s} \quad (8)$$

Finally, a correlation is obtained from which it is obvious that the detected intensity ratio $R^{(0)}$ is dependent on the pH-dependent function $R^{(z_s)} = f_{662.5}^{(z_s)}/f_{587.5}^{(z_s)}$ at the scanning depth z_s, and on an exponential expression describing the alteration of the intensity ratio due to the wavelength-dependent light attenuation:

$$R^{(0)}(\mathrm{pH}, z_s) = R^{(z_s)}(\mathrm{pH})\, e^{-c(\varepsilon_{662.5}-\varepsilon_{587.5}) z_s} \quad (9)$$

It is additionally obvious from this equation that the detected intensity ratio, $R^{(0)}$, should become larger with the factor $e^{-c(\varepsilon_{662.5}-\varepsilon_{587.5}) z_s}$ with increasing scanning depth z_s. This is due to the fact, that according to the Rayleigh scattering $\varepsilon_{587.5}$ is larger than $\varepsilon_{662.5}$.

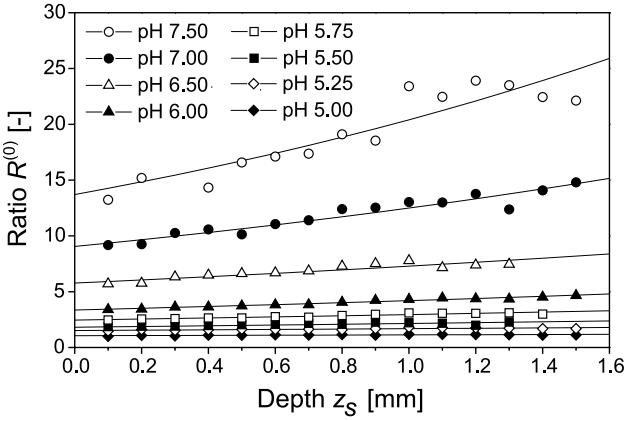

Fig. 4. Measured intensity ratios as a function of scanning depth and pH in comparison with fitted curves according to Eq. (9).

In the following, the proposed mathematical model shall be verified. According to Eq. (9), the detected intensity ratio $R^{(0)}$ increases with a constant factor with increasing scanning depth z_s. Thus, the parameters of Eq. (9) ($R^{(z_s)}$ and $-c(\varepsilon_{662.5}-\varepsilon_{587.5})$) were determined by fitting a series of experimentally obtained intensity ratios, $R^{(0)}$, originating from various scanning depths and gathered from alginate beads which were adjusted to different pH values, to this equation. Fig. 4 shows the respective experimental values as well as the fitted curves. The values for $R^{(z_s)}$ and $-c(\varepsilon_{662.5}-\varepsilon_{587.5})$, obtained by the fitting, are presented in Table 1 . It can be seen from this table that, in contrast to the proposed model, the exponents of the exponential expression (the factors $-c(\varepsilon_{662.5}-\varepsilon_{587.5})$) are not constant. Instead, they grow with increasing pH. This discrepancy between the proposed

Table 1
Values for $R^{(z_s)}$ and $-c(\varepsilon_{662.5}-\varepsilon_{587.5})$ obtained by fitting Eq. (9) to the experimental curves presented in Fig. 4

pH	$R^{(z_s)}$	$-c(\varepsilon_{662.5}-\varepsilon_{587.5})$
7.50	13.44	0.40
7.00	9.07	0.32
6.50	5.79	0.23
6.00	3.35	0.22
5.75	2.46	0.18
5.50	1.82	0.17
5.25	1.51	0.10
5.00	1.05	0.07

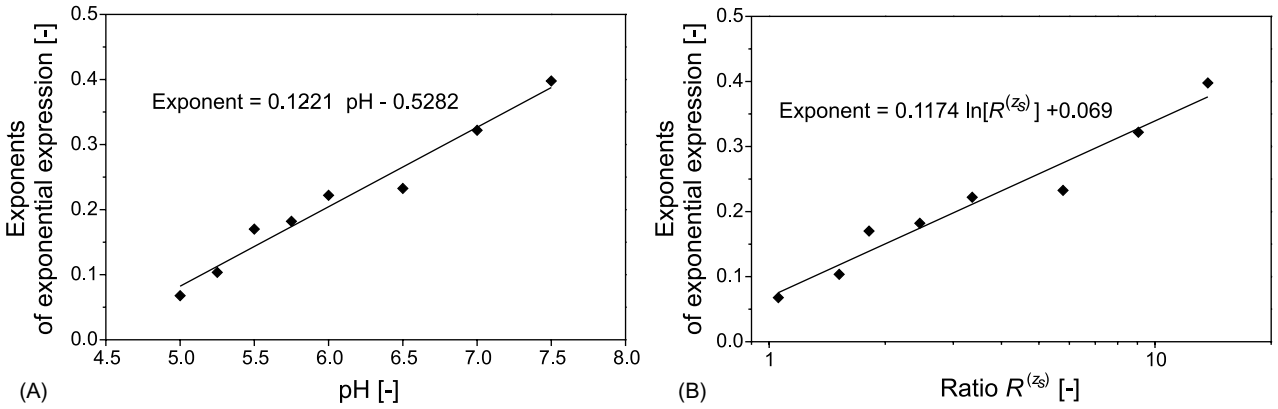

Fig. 5. Correlations between the exponents of the exponential expression $-c(\varepsilon_{662.5} - \varepsilon_{587.5})$ and pH (A) and $R^{(z_s)}$ (B), respectively.

model and the experimentally observed behavior indicates that the developed model does not hold true. It is possible that either an underlying assumption is not correct or that an additional effect has to be included in the model equations. Thus, further investigations were necessary.

3.2.2. Hypothesis 2: wavelength-dependent attenuation and partial re-absorption of emitted light

From the values presented in Table 1, it can be seen that the exponents of the exponential expressions are correlated in a certain way with the intensity ratio $R^{(z_s)}$ and with the pH at the scanning depth z_s, since $R^{(z_s)}$ is a function of the pH. The according relationships are presented in Fig. 5, where the experimentally obtained exponents of the exponential expression are plotted versus the respective pH and $R^{(z_s)}$ values. The correlations describe the exponent of Eq. (9) as a linear function of pH and as a logarithmic function of the intensity ratio $R^{(z_s)}$. The pH-dependent exponents demonstrate that the observed augmentation of the detected intensity ratio with increasing scanning depth is not only a function of the scanning depth, as it was proposed in hypothesis 1, but also a function of the pH. A potential explanation for this phenomenon could be a partial re-absorption of emitted light on its way through the particle by the fluorophore itself [35]. Re-absorption of emitted light is enabled if the fluorophore's absorption and emission spectra overlap. Absorption and emission spectra (excitation at 568 nm) of the here applied dye SNARF-4F are given in Fig. 6 for pH 5 and 7.5. It is obvious from this figure that indeed light emitted at lower wavelengths can be re-absorbed. Due to the fact that the fluorophore's absorption and emission spectra alter with changing pH, the degree of re-absorption is also dependent on pH.

The correlations, presented in Fig. 5, were obtained from measurements in alginate beads, which were all preset to a different but constant pH value in the whole bead. Thus, the correlation in Fig. 5B can be used to derive an expression which represents the measured intensity ratio, $R^{(0)}$, as a function of the intensity ratio profile in the alginate bead, $R(z)$, and as a function of the scanning depth z_s. The expression obtained after replacing the exponent in Eq. (9), $-c(\varepsilon_{662.5} - \varepsilon_{587.5})$, with the logarithmic correlation from Fig. 5B is:

$$R^{(0)} = R^{(z_s)}\, e^{(0.1174 \ln R(z) + 0.069)z} \tag{10}$$

and after rearranging

$$R^{(0)} = R^{(z_s)} \underbrace{e^{(0.1174 \ln R(z))z}}_{a} \underbrace{e^{0.069z}}_{b} \tag{11}$$

In Eq. (11), term b represents the wavelength-dependent change of the intensity ratio $R^{(z_s)}$ along the path of the light according to Rayleigh scattering. Term a denotes the change of the intensity ratio due to the $R(z)$-dependent re-absorption (i.e. pH-dependent) of the emitted light by the fluorophore. If the pH is constant throughout the whole bead, which means that $R(z) = \text{constant} = R^{(z_s)}$, then Eq. (11) can be rearranged to:

$$R^{(0)} = R^{(z_s)1+0.1174z}\, e^{0.069z} \tag{12}$$

Thus, if the pH is constant in the particle, then the intensity ratio at the scanning depth z_s, $R^{(z_s)}$, can be determined from the measured intensity ratio $R^{(0)}$ by using Eq. (12).

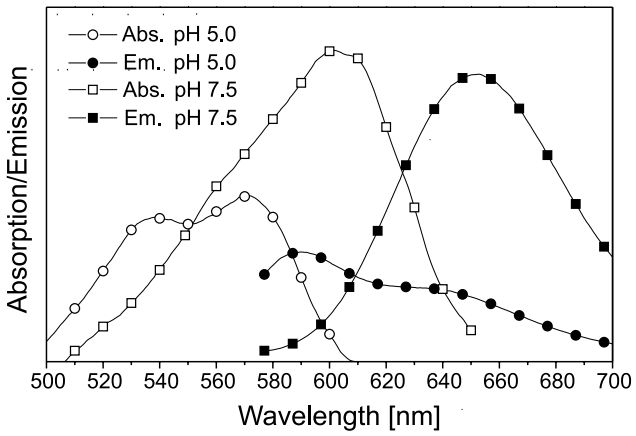

Fig. 6. Absorption spectra (□, ○) and emission spectra (■, ●), obtained with excitation at 568 nm, of a buffer solution (89.5 mM MES, 17.9 mM TRIS) containing 3.6 μM SNARF-4F at pH 5.0 (●, ○) and pH 7.5 (■, □).

In dynamic experiments, however, the pH in the particles might change over time, which means that the intensity ratio profile, $R(z)$, is not constant. In this case, Eq. (11) changes after integration to:

$$R^{(0)} = R^{(z_s)}\, e^{\int_0^{z_s}(0.1174 \ln R(z))\,dz}\, e^{0.069z} \quad (13)$$

Thus, for the determination of the intensity ratio at the scanning depth z_s, $R^{(z_s)}$, the whole profile of the intensity ratio, $R(z)$, and thus also the pH profile, pH(z), above the current scanning plane have to be known. This is, however, exactly the quantity the measurement is actually aiming at.

4. Discussion

The dependence of the measured signal $R^{(0)}$ on the usually unknown pH profile, pH(z), (and $R(z)$, respectively) above the scanning plane, ends up in the fact that the pH measurement in macroscopic large objects, at least with the fluorophores and the fluorophore concentrations, which were used in our work and in the work of Spiess and Kasche [24], is not possible. This is due to the fact, that the (usually unknown) pH profile above the scanning plane falsifies the actually measured signal and thus, strongly biased results are obtained. In the following, the extent of the distortion caused by the pH-dependent re-absorption will be demonstrated.

In two exemplary scenarios, illustrated in Fig. 7, an optical slice is scanned at depth $z = 1.5$ mm. In both scenarios, the pH at the scanning depth is assumed to be 7.0 (i.e. $R^{(z_s)} = 9$). In scenario 1, a constant pH is present in the whole bead, whereas in scenario 2, a linear pH profile pH(z) is present in the bead above the scanning plane with pH 5 at $z = 0$. This arbitrarily chosen pH profile, characterizing scenario 2, is given by the following equation with z in mm:

$$\mathrm{pH}(z) = \tfrac{4}{3}z + 5 \quad (14)$$

This pH profile pH(z) can subsequently be transferred into a profile of intensity ratios, $R(z)$, by using a combination of the two correlations in Fig. 5:

$$R(z) = e^{(0.1221\mathrm{pH}(z) - 0.5972)/0.1174} \quad (15)$$

In the following, the intensity ratios $R^{(0)}$, which would be detected at $z = 0$, are calculated for both scenarios. The intensity ratio $R^{(0)}$ of scenario 1 is obtained with Eq. (12). The calculation results in an intensity ratio $R^{(0)}$ of 14.7. The intensity ratio, which is obtained in scenario 2, is calculated with the Eqs. (13)–(15). The computation, which can be performed with an appropriate software package (e.g. Maple), results in an intensity ratio $R^{(0)}$ of 12.2. The comparison of the two resulting intensity ratios shows that, although in both scenarios the same intensity ratio (and respectively, the same pH) is present at the scanning depth z_s, the value, obtained for the constant pH profile, is approximately 20% larger than the value for the linear pH profile.

It is obvious from this difference that the pH above the scanning plane has a strong impact on the measured intensity ratio $R^{(0)}$. Even worse, the deviation of 20% cannot be regarded as a statistical, normally distributed error. It rather represents a biased result with a systematic error. As a consequence, the method cannot be applied when the pH above the scanning plane is unknown which is normally the case in dynamic experiments. The application of this method is therefore restricted to cases when it is known that a constant pH is present throughout the bead. In this case, Eq. (12) can be used for the calculation of $R^{(z_s)}$.

For other cases, when an unknown pH profile is present in the bead, it has to be distinguished between dynamically changing pH profiles or stationary pH profiles. If a stationary pH profile is ensured by the experimental setup, then the pH profile inside the object can be determined by incrementally scanning the particle in z-direction. The obtained intensity ratio of each scanning step can then be corrected with previously gathered ratios. In the case of dynamically changing pH profiles, this incremental procedure is only possible if the time scale of the dynamic pH change is much lower then the time needed for the incremental scanning process.

5. Conclusions

To date, both, experimental investigations of protein adsorption processes and mathematical models describing such processes indicate that the pH in the absorbent

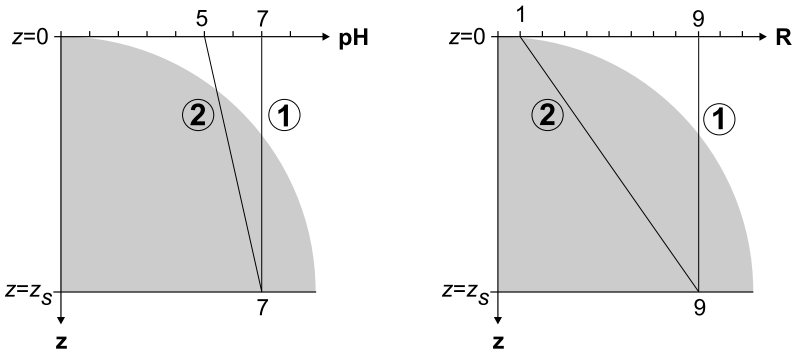

Fig. 7. Exemplary scenarios for illustration of systematic error.

particles might be the key factor for an improved understanding of these chromatographic processes. Therefore, in the present study, a new technique was proposed to measure pH in macroscopic large particles, based on confocal laser scanning microscopy. The application of CLSM based methods for pH measurement in macroscopic large objects, however, revealed an apparent depth dependence of the ratiometric signal. The ratiometric signal, originating from the scanning depth, is distorted on its way through the macroscopic large object. By a model-based approach, two phenomena were identified to cause this distortion: firstly, the wavelength-dependent attenuation of the emitted light according to the Rayleigh scattering and secondly, the pH-dependent re-absorption of emitted light by the fluorophore. With the derived model, it was shown that the ratiometric pH measurement technique, as it was applied in our work and in the work of Spiess and Kasche [24], leads to negatively biased results during dynamic pH measurements in macroscopic large objects.

The re-absorption phenomenon, being mainly responsible for the negative bias, however, can be decreased by a reduction of the dye concentration, resulting from a decreased re-absorption probability of emitted light. A reduction of the dye concentration is associated with a decrease in the detected light intensities (here at 587.5 and 662.5 nm). Since according to the absorption spectra and emission spectra presented in Fig. 6, basically only light at the lower intensity is re-absorbed, the error in the final measurement variable (i.e. the ratio of the two light intensities) can therefore be reduced by decreasing the dye concentration. However, before being able to use lower dye concentrations several measures have to be taken in order to ensure that enough fluorescence signal is obtained especially from increased scanning depths. Such measures are, for example, an increase of the collection window size, the use of a different beamsplitter with a higher transmission of fluorescent light, the use of dyes with higher quantum yields and also the use of smaller beads or beads from more transparent materials causing fewer signal losses due to scattering. It is important to note however, that although re-absorption (and consequently the bias in the ratiometric measurement variable) is reduced at lower dye concentrations, the re-absorption effect and the bias themselves do not completely diminish. The only possibility to completely overcome this problem is given by the application of a specific dual-emission fluorescent dye which exhibits a Stokes shift which is large enough to ensure that the absorption and emission spectra do not overlap. However, to the best of our knowledge such dye is not on the market. The same beneficial effect of separated absorption and emission spectra can also be achieved with the selection of two different fluorescent dyes whose absorption and emission spectra are separated enough. However, with the application of two different dyes, the discussed disadvantages come into effect again. Besides the outlined modifications to cope with the re-absorption effect, also by the application of modern techniques such as fluorescence lifetime or multiphoton fluorescence microscopy some of the outlined problems associated with the spatially resolved dynamic pH measurement in macroscopic large objects could be partially circumvented, but also sets of new experimental artifacts have to be avoided with these techniques.

List of symbols

c	concentration of absorbing species
f	function characterizing the pH-dependent emission of the dye at a distinct wavelength
h	function characterizing microscopic and fluorophore parameters
I	fluorescence intensity
n	refractive index
NA	numerical aperture
R	ratio of fluorescence intensities
R_a	axial resolution of objective lens
R_l	lateral resolution of objective lens
z	z position
z_s	scanning depth

Greek letters

ε	absorptivity coefficient
λ	wavelength

Subscripts

587.5	emission between 585 and 590 nm
662.5	emission between 660 and 665 nm
ex	excitation

Superscripts

(0)	scanning depth 0
(z_s)	scanning depth z_s

Acknowledgements

The authors gratefully acknowledge the financial support of the Deutsche Forschungsgemeinschaft (DFG) within the Collaborative Research Center (SFB) 540. We also wish to thank Dipl.-Phys. Sebastian Schuler, 3. Physikalisches Institut, Stuttgart University, for extended discussions concerning the optical phenomena and for critical reviewing of the manuscript. Furthermore, we thank Dr. Stephano Di Fore, Department of Molecular Biotechnology, RWTH Aachen University, for his help and assistance with the spectrofluorimeter.

References

[1] A. Ljunglöf, J. Thömmes, J. Chromatogr. A 813 (1998) 387.
[2] T. Linden, A. Ljunglöf, M.-R. Kula, J. Thömmes, Biotechnol. Bioeng. 65 (1999) 622.
[3] M. Malmsten, K. Xing, A. Ljunglöf, J. Colloid. Interf. Sci. 220 (1999) 436.

[4] A. Ljunglöf, M. Larsson, K.-G. Knuuttila, J. Lindgren, J. Chromatogr. A 893 (2000) 235.
[5] S.R. Dziennik, E.B. Belcher, A.M. Lenhoff, Presentation at the 20th International Symposium on the Separation and Analysis of Proteins, Peptides and Polynucleotides (ISPPP 2000), Ljubljana, Slovenia, 5–8 November 2000, Paper L-102.
[6] M. Heinemann, T. Wagner, B. Doumèche, M.B. Ansorge-Schumacher, J. Büchs, Biotechnol. Lett. 24 (2002) 845.
[7] J. Hubbuch, T. Linden, E. Knieps, J. Thömmes, M.-R. Kula, Biotechnol. Bioeng. 80 (2002) 359.
[8] T. Linden, A. Ljunglöf, L. Hagel, M.-R. Kula, J. Thömmes, Sep. Sci. Technol. 37 (2002) 1.
[9] U. Reichert, T. Linden, G. Belfort, M.-R. Kula, J. Thömmes, J. Memb. Sci. 199 (2002) 161.
[10] S.R. Dziennik, E.B. Belcher, G.A. Barker, M.J. DeBergalis, S.E. Fernandez, A.M. Lenhoff, Proc. Natl. Acad. Sci. U.S.A. 100 (2003) 420.
[11] M.A. Fernandez, G. Carta, J. Chromatogr. A 746 (1996) 169.
[12] M.A. Fernandez, G. Carta, J. Chromatogr. A 746 (1996) 185.
[13] A. Johnston, M.T.W. Hearn, J. Chromatogr. 557 (1991) 335.
[14] H. Yoshida, M. Yoshikava, T. Kataokal, AIChE J. 40 (1994) 2034.
[15] A.I. Liapis, J. Chromatogr. A 921 (2001) 135.
[16] B.A. Grimes, A.I. Liapis, J. Colloid Interf. Sci. 248 (2002) 504.
[17] X. Hu, D.D. Do, Q. Yu, Chem. Eng. Sci. 47 (1992) 141.
[18] D.P. Taylor, J. Slattery, A.C. Leopold, Physiol. Plant. 97 (1996) 35.
[19] M. Opas, Trends Cell Biol. 7 (1997) 75.
[20] M. Weinlich, U. Heydasch, M. Starlinger, R.K.H. Kinne, Z. Gastroenterol. 35 (1997) 263.
[21] R.B. Silver, Methods in Cell Biology, vol. 56, Academic Press, San Diego, New York, 1998.
[22] A. Takahashi, Y. Zhang, V.E. Centonze, B. Herman, BioTechniques 30 (2001) 804.
[23] F. Fergg, Nitratreduktion mittels in Polyvinylalkohol-Hydrogelpellets immobilisierten Bimetallkatalysatoren, Ph.D. Thesis, TU Hamburg-Harburg, 1999.
[24] C.A. Spiess, V. Kasche, Biotechnol. Progr. 17 (2001) 294.
[25] K.I. Draget, G. Skjåk-Bræk, O. Smidsrød, Int. J. Biol. Macromol. 21 (1997) 47.
[26] W.R. Gombotz, S.F. Wee, Adv. Drug. Deliver Rev. 31 (1998) 267.
[27] R.P. Haugland, Handbook of Fluorescent Probes and Research Products, Molecular Probes Inc., Eugene, 1996.
[28] X. Liu, Z. Diwu, W.-Y. Leung, Bioorg. Med. Chem. Lett. 11 (2001) 2903.
[29] K. Carlsson, N. Åslund, Appl. Opt. 26 (1987) 3232.
[30] T.D. Visser, F.C.A. Groen, G.J. Brakenhoff, J. Microsc. 163 (1991) 189.
[31] J.B.T.M. Roerdink, M. Bakker, J. Microsc. 169 (1993) 3.
[32] A. Liljeborg, Three Dimensional Microscopy, Image Acquisition and Processing. Part II. Proceedings SPIE 2655 (1996) 11.
[33] K. Mütze, ABC der Optik, Verlag Werner Dausien, Hanau, 1961.
[34] J.R. Lakowicz, Principles of Fluorescence Spectroscopy, Kluwer Academic Publishers, New York, 1999.
[35] P. van Oostveldt, S. Bauwens, J. Microsc. 158 (1990) 121.